Letter

X-ray two-beam topography for quantitative derivation of phase shift by crystalline dislocations

Yoshiki Kohmura,[1] Kenji Ohwada,[2] Nobuki Kakiuchi,[3] Kei Sawada,[1] Tadaaki Kaneko,[3] Jun'ichiro Mizuki,[3] Masaichiro Mizumaki,[4] Tetsu Watanuki,[2] and Tetsuya Ishikawa[1]

[1]*RIKEN SPring-8 Center, 1-1-1 Kouto, Sayo-gun, Sayo-cho, Hyogo 679-5148, Japan*

[2]*Synchrotron Radiation Research Center, Kansai Photon Science Institute, Quantum Beam Science Research Directorate, National Institutes for Quantum Science and Technology, SPring-8, 1-1-1 Kouto, Sayo, Hyogo 679-5148, Japan*

[3]*School of Science and Technology, Kwansei Gakuin University, 1 Gakuen Uegahara, Sanda, Hyogo 669-1330 Japan*

[4]*Japan Synchrotron Radiation Research Institute, SPring-8, 1-1-1 Kouto, Sayo, Hyogo 679-5198, Japan*

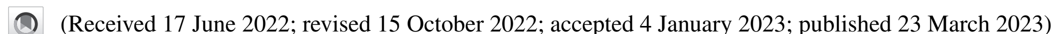

(Received 17 June 2022; revised 15 October 2022; accepted 4 January 2023; published 23 March 2023)

Quantitative evaluation of crystalline dislocations is gaining importance in order to realize functional materials with ultimate performance. X-ray topography has been an important tool to evaluate the crystalline dislocations in bulk in a large volume, but the research up to now lacks the analysis to derive the phase at the image plane and such a situation prevents us from obtaining knowledge of lattice planes around the crystalline dislocations. Here we report a method that enables us to obtain such knowledge in a crystal using an x-ray two-beam topography at the kinematical diffraction regime. It can quantitatively derive the phase shift by the Bragg reflection around the crystalline dislocations. We observed an x-ray vortex wave field from a silicon carbide crystal containing a screw dislocation which almost perfectly agrees with simulations. This method will clarify the distribution and network of the threading screw dislocations and other dislocations in a large field of view.

DOI: 10.1103/PhysRevResearch.5.L012043

I. INTRODUCTION

The importance of crystal lattice engineering is growing rapidly. For example, threading screw dislocations (TSDs) significantly reduces the breakdown voltage that can be raised by excluding TSDs when silicon carbide (SiC) crystals are utilized in high-power electronic devices [1]. The TSDs were traditionally observed by x-ray topography [1–3], scanning microbeam diffraction methods, and reticulography [4]. These methods, however, did not provide any clear knowledge of the lattice planes around the TSDs. Therefore, the details of the network of TSDs in a large field of view (FOV) could not be clarified by these measurements. We propose here a method of x-ray two-beam topography by which we can determine the phase at the detector plane that is directly related to the deformation of lattice planes around dislocations. The large FOV available by our method provides the knowledge of the network of TSDs and other dislocations, a key factor for the industry to reduce the density of TSDs in SiC crystals.

Our two-beam x-ray topography uses Bragg reflection from an offset area of a TSD as the reference, instead of adding a crystal as in the case of the Moiré topography [5]. We also use the Bragg reflected wave field from a crystal containing dislocations at a kinematical diffraction condition by setting the crystal at the off-Bragg condition. This method is an analog of the weak-beam method in the diffraction contrast imaging of electron microscopes [6]. This condition reduces the complexity of multiple diffraction around dislocations much more than the case of dynamical diffraction condition. The Bragg reflected wave fields can be simulated by the Fourier transform of the electron density in the crystal without such difficulty as faced in the dynamical diffraction condition [7,8].

Our technique enables us to quantitatively derive the phase shift by the Bragg reflection from the crystalline dislocations. This was exemplified by observing a fork pattern in the experimental interferogram which manifested the generation of an x-ray vortex wave field, an analog of the visible one [9,10] with various applications [11–14], from a crystal containing a screw dislocation. The pattern agreed well with the computer simulation. Without iteration calculations, this method solves the phase problem at the detector plane which other methods using only one beam suffer. While transmission electron microscope and Bragg coherent diffractive imaging [15] can provide much higher spatial resolution than our case of around 4 μm or so, our method has a complementary role due to a much relaxed sample size constraint, up to millimeter scale, of bulk crystalline specimens. The spatial resolution of around 4 μm or so is limited mainly by the doubled core radius of the TSD, calculated for the present experimental condition. This method will clarify the distribution and the network of TSDs and other dislocations in a large FOV.

II. EXPERIMENTAL SETUP

For the two-beam topography experiment, we utilized a large 4H-SiC wafer with a size of approximately

Published by the American Physical Society under the terms of the Creative Commons Attribution 4.0 International license. Further distribution of this work must maintain attribution to the author(s) and the published article's title, journal citation, and DOI.

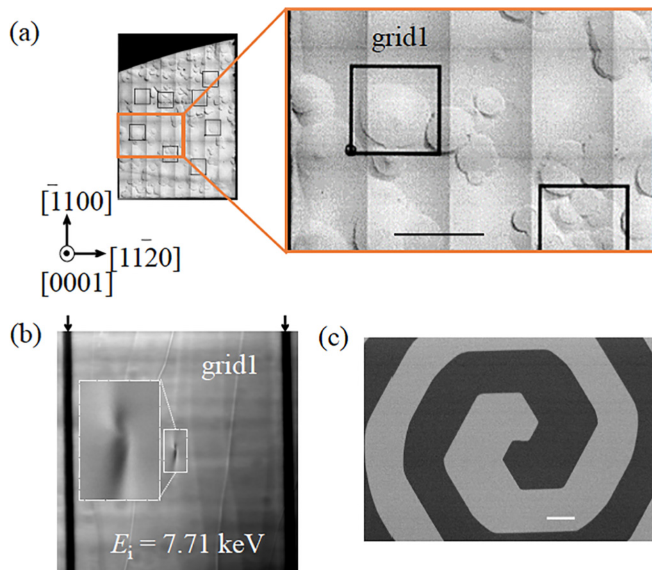

FIG. 1. (a) Nomarski differential interference contrast microscope image of the surface of SiC wafer after Si-vapor thermal etching. A quasicircular edge of the etched region was observed around TSDs with an approximate diameter of 1 mm. (b) X-ray topograph image around the center of grid 1 shown in Fig. 1(a). Black arrows show parts of grid 1. (c) LEECC image at the focus condition observed at the center of grid 1, where a spiral pattern corresponding to the TSD is clearly observed. The scale bars are (a) 1 mm and (c) 1 μm.

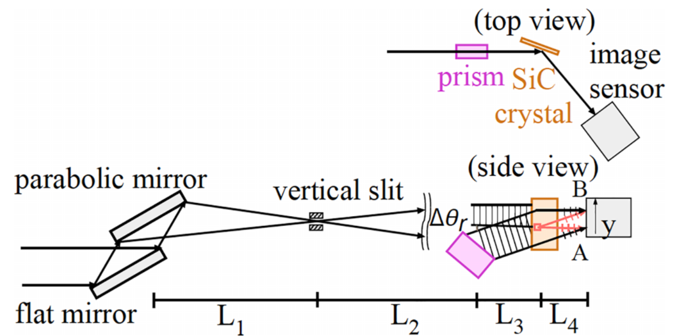

FIG. 2. Schematic diagram of a wave-front dividing two-beam interferometer with a diamond prism splitter. The interference fringes are formed at the overlap of x rays due to the refraction angle of $\Delta\theta_r$ by the prism. The images of TSDs in the interferogram are formed at positions *A* and *B*. Here L_1, L_2, L_3, and L_4 correspond to distances between the parabolic mirror-vertical slit, vertical slit-prism, prism-SiC crystal, and SiC crystal-image sensor of 17.3, 44.3, 3.6, and 0.07 m, respectively.

$10 \times 10 \times 0.2$ mm^3 containing TSDs. The stress of lattice planes was eliminated and clean surfaces at an atomic level were obtained by the Si-vapor thermal etching at a temperature of 1800 °C. For alignment, square grids of 1×1 mm^2 were formed around the cores of TSD by laser processing [Fig. 1(a)]. The x-ray topograph image shown in Fig. 1(b) shows that the core of TSD, elongated due to the grazing incidence, appears dark at the Bragg condition. By etching the surface of the wafer, the existence of TSDs on the wafer was confirmed by their screw features in a low-energy electron channeling contrast (LEECC) image [Fig. 1(c)].

To measure the phase distribution in the reflected wave downstream of a SiC crystal, we constructed an x-ray wave-front dividing interferometer [16–18] at an undulator beamline, BL29XUL [19] in SPring-8, Japan. The gap of the undulator was set to be 12.21 mm to equalize the first-order harmonics to be 7.71 keV. The x-ray beam energy from the in-vacuum undulator was monochromatized by a silicon-double-crystal monochromator in the transport channel. To avoid the vertical vibrations of the light source and monochromator crystals, we devised a stable and reliable interferometer as follows.

This interferometer uses a one-dimensionally focused x-ray beam in the vertical direction which passes through a slit at the focal plane to realize a stable virtual source. To focus, we used the parabolic mirror set at the second part of the double total reflection mirrors in the transport channel [20]. The grazing incidence angle was set to be around 1.3 mrad to realize $F \simeq 12.7$ m and realize focusing at around $L_1 = 17.3$ m from this mirror. By scanning the 10-μm-width slit, the vertical focused beam size was measured to be around 15 μm (FWHM). In this focal spot, we placed a 10-μm-width slit and realized a bright virtual source.

The wave-front dividing two-beam x-ray interferometer consists of a diamond prism, set at a location of $L_2 = 44.3$ m from this 10-μm-width slit, which refracts a part of the wave field in the vertical direction perpendicular to the horizontal Bragg reflection plane of the SiC crystal (Fig. 2). One of the wave fields irradiates an offset position from the center of the TSD, working as a reference wave which is approximated by a plane wave, while the other wave field irradiates the center of the TSD, which receives a specific phase shift (Fig. 2). The grazing incidence angle on the prism was chosen to be approximately equal to 17° to realize the refraction angle of $\Delta\theta_r = 38$ μrad and the interference fringe spacing of $d_f = \lambda/\Delta\theta_r = 4.2$ μm, resolvable by our x-ray image sensor. The distance between the prism and crystal was chosen to be $L_3 = 3.6$ m so that the width of the interference region, $L_3\Delta\theta_r = 140$ μm, is large enough to cover the lattice planes around the TSD.

X-ray image sensor is composed of a scintillator, a lens coupled visible light optical system, and a scientific complementary metal-oxide semiconductor camera [21] with a 20× lens with an effective pixel size of 0.325 μm. It was placed downstream of the SiC crystal with the distance between the crystal and image sensor $L_4 = 7$ cm as shown in Fig. 2. The distance L_4 was carefully chosen so that the images of TSDs passing through the two paths are clearly separated in the vertical direction at *A* and *B* in the interferogram (see Fig. 2). Our method enables us to investigate the nature of TSDs without severe thickness and size limitations of the samples.

III. COMPUTER SIMULATION

We now perform a kinematical diffraction simulation of the Bragg reflected x-ray wave field downstream of a SiC crystal, which contains a TSD on the (0004) plane. For this

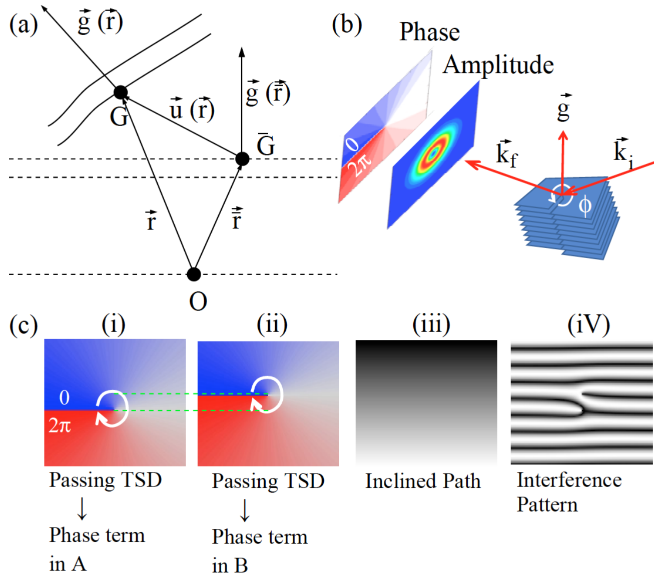

FIG. 3. (a) Schematic diagram showing the definitions of the variables used for deriving Eq. (1). Here $\bar{G}$ on the dotted line and G on the solid line correspond to points on a perfect lattice and a deformed lattice, respectively, and $\vec{g}(\vec{r})$, $\vec{u}(\vec{r})$, and $\vec{r}$ correspond to the reciprocal lattice vector, displacement vector, and atomic positions on the displaced lattice, respectively. (b) Summary of the kinematical diffraction simulation. Here $k_{\rm i}$ and $k_{\rm f}$ are incident and exit waves and ϕ is the azimuthal angle around TSD. The calculated phase and amplitude of the x-ray Bragg reflected wave field downstream of a crystal with a TSD are shown on the left, exhibiting a donut intensity profile and a spiral phase distribution with a phase jump of 2π. They indicate that an x-ray vortex is generated at the reciprocal space. A TSD on SiC(0004) plane was assumed and the number of the atoms in the calculated model was $101 \times 101 \times 101$. (c) Phase terms in (i) pass A, (ii) pass B and (iii) both pass A and B as shown in Fig. 2. (iv) Simulated interferogram.

simulation, the scattering factor

$$S(\vec{q}\,) \propto \int \exp[-2\pi i\vec{g}(\vec{r}\,)\cdot\vec{u}(\vec{r}\,)]\exp(-2\pi i\vec{q}\cdot\vec{r}\,)dv \qquad (1)$$

is calculated, where $\vec{q}$, $\vec{g}(\vec{r}\,)$, $\vec{u}(\vec{r}\,)$, and $\vec{r}$ correspond to a scattering vector, a reciprocal lattice vector, the displacement vector, and an atomic position of deformed crystal lattice, respectively [see the caption of Fig. 3(a) for details]. The displacement vector $\vec{u}(\vec{r}\,)$ is parallel to $\vec{g}(\vec{r}\,)$, with $\vec{g}(\vec{r}\,)\cdot\vec{u}(\vec{r}\,) = \phi$ around the TSD. The simulated result shows a destructive interference in the Bragg reflected beam which induces an x-ray vortex wave field at the reciprocal space, as shown in Fig. 3(b). The interferogram in Fig. 3(c iv) shows two reversed Y-forked patterns separated by an amount of shear $L_4\Delta\theta_r$.[1]

[1]Assuming phase term due to TSD of $\Theta(y)$, reflected amplitude of $a_A = \exp(i\Theta(y)) + \exp(-2\pi iy/d_f)$ through pass A and $a_B = \exp(i\Theta(y - L_4\Delta\theta_r)) \times \exp(-2\pi iy/d_f) + 1$ through pass B are obtained. See Fig.2 for the definition of axis y.

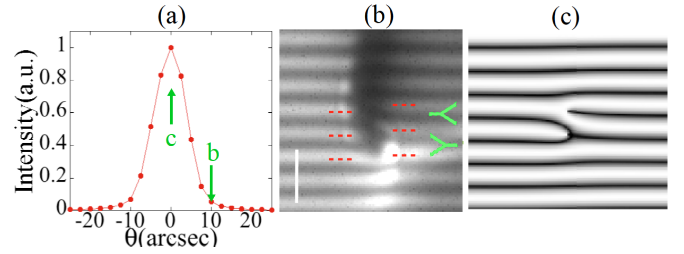

FIG. 4. (a) Measured rocking curve at a region shifted from the center of TSD in grid 1 in Fig. 1(b). (b) Interferograms obtained at the grazing incidence angle denoted by b in (a), corresponding to the off-Bragg condition (offset angle $\Delta\theta = 10''$). The measured reflectivity at angle b was about 5.5% compared to that of the Bragg peak. Two Y-shaped fork patterns with reversed orientations were observed which are separated by the amount of shear. The exposure time in (b) is 20 s and the scale bar is 10 µm. (c) Simulated interferogram in the kinematical diffraction regime.

IV. EXPERIMENTAL RESULT

The observed rocking curve, measured away from the core of the TSD in grid 1 in Fig. 1(b), is shown in Fig. 4(a). The measured Darwin width is approximately $9''$. Interferograms are recorded by setting the incidence angle at the off-Bragg condition with $\Delta\theta = 10''$. It realizes a weak-beam condition with the measured reflectivity of 5.5% relative to the Bragg peak and the multiple diffraction effect is negligible, as discussed in the next paragraph. The interferogram showed two Y-shaped fork patterns with reversed orientations, which are separated by the amount of shear [see Fig. 4(b)]. It agrees well with the simulation in the kinematical diffraction regime shown in Fig. 4(c). It indicates that an x-ray vortex with a topological charge of 1 is formed in the Bragg reflected wave field. It clearly showed that our two-beam topography enables us to quantitatively derive the phase shift by the Bragg reflection from the screw dislocation as simulated by Eq. (1) and Fig. 3(b). The radius of the two dark spots appearing in the interferogram, corresponding to the core of the TSDs, is 2 µm. The spatial resolution for detecting TSDs is estimated by doubling this radius to be around 4 µm.

We then check whether the offset angle selected in the experiment ($\Delta\theta = 10''$) with a measured x-ray reflectivity of $R \simeq 0.055$ [Fig. 4(b)] is appropriate for suppressing the multiple diffraction effect. The off-Bragg condition reduces the multiple diffraction and diminishes the Pendellösung effect on the reflectivity. When the amplitude reflectivity r of a single lattice and negligible x-ray attenuation inside the crystal are assumed, differences of $R = r^2(1 + r^2 +)^2 \simeq 0.055$ (for multiple reflections) and $r^2 \simeq 0.052$ (calculated from R) are extremely small, which guarantees the negligible contribution of multiple reflection. Moreover, the multiple diffraction is excluded in the proximity of the core of the TSD due to the huge inclination angle variation of lattice planes.

V. CONCLUSION

We have proved that our x-ray two-beam topography is useful for quantitative derivation of the phase shift by the Bragg reflection from the crystalline dislocation at a

kinematical diffraction condition. It enables us to detect an x-ray vortex wave field formed at a crystal containing a screw dislocation. The experimental result agreed well with a simulation and showed a large potential of x-ray two-beam topography to precisely elucidate the lattice planes around crystalline dislocations without severe limitation of crystal size and without an additional crystal for reference. This method will clarify the distribution and the network of threading screw dislocations and other dislocations in a large field of view and should play an important role in the reduction of threading screw dislocations dramatically in the near future.

ACKNOWLEDGMENTS

This research was supported by KAKENHI (Grant No. 22109005) from JSPS of Japan. The use of BL29XUL at SPring-8 was supported by RIKEN and JASRI under Proposal No. 2018A1169.

[1] U. Zimmermann, J. Osterman, D. Kuylenstierna, A. Hallen, A. O. Konstantinov, W. M. Vetter, and M. Dudley, Material defects in 4*H*-silicon carbide diodes, J. Appl. Phys. **93**, 611 (2003).

[2] E. V. Suvorov and I. A. Smirnova, Diffraction image of screw dislocations in X-ray section topography methods, J. Surf. Investig. X-Ray **5**, 1189 (2011).

[3] Y. Yamaguchi and H. Matsuhata, Threading screw dislocations in 4H-SiC wafer observed by the weak-beam method in Bragg-case x-ray topography, J. Electron. Mater. **39**, 715 (2010).

[4] A. R. Lang and A. P. W. Makepeace, Reticulography: A simple and sensitive technique for mapping misorientations in single crystals, J. Synchrotron Radiat. **3**, 313 (1996).

[5] A. R. Lang, X-ray Moiré topography of lattice defects in quartz, Nature (London) **220**, 652 (1968).

[6] D. A. Williams and C. B. Carter, *Transmission Electron Microscopy* (Plenum, New York, 1996), Chap. 26.

[7] S. Takagi, Dynamical theory of diffraction applicable to crystals with any kind of small distortion, Acta Cryst. **15**, 1311 (1962); A Dynamical Theory of Diffraction for a Distorted Crystal, J. Phys. Soc. Jpn. **26**, 1239 (1969).

[8] D. Taupin, Théorie dynamique de la diffraction des rayons X par les cristaux déformés, Bull. Soc. Fr. Min. Cristallogr. **87**, 469 (1964).

[9] M. Padgett, J. Courtial, and L. Allen, Light's orbital angular momentum, Phys. Today **57**(5), 35 (2004).

[10] M. Katoh, M. Fujimoto, H. Kawaguchi, K. Tsuchiya, K. Ohmi, T. Kaneyasu, Y. Taira, M. Hosaka, A. Mochihashi, and Y. Takashima, Angular Momentum of Twisted Radiation from an Electron in Spiral Motion, Phys. Rev. Lett. **118**, 094801 (2017).

[11] S. Hell, Toward fluorescence nanoscopy, Nat. Biotechnol. **21**, 1347 (2003).

[12] A. L. Porta and M. D. Wang, Optical Torque Wrench: Angular Trapping, Rotation, and Torque Detection of Quartz Microparticles, Phys. Rev. Lett. **92**, 190801 (2004).

[13] Y. Kohmura, K. Sawada, M. Mizumaki, K. Ohwada, T. Watanuki, and T. Ishikawa, X-ray microscope for imaging topological charge and orbital angular momentum distribution formed by chirality, Opt. Express **28**, 24115 (2020).

[14] R. Fickler, R. Lapkiewicz, M. Huber, M. P. J. Lavery, M. J. Padgett, and A. Zeilinger, Interface between path and orbital angular momentum entanglement for high dimensional photonic quantum information, Nat. Commun. **5**, 4502 (2014).

[15] J. N. Clark, J. Ihli, A. S. Schenk, Y-Y Kim, A. N. Kulak, J. M. Campbell, G. Nisbet, F. C. Meldrum, and I. K. Robinson, Three-dimensional imaging of dislocation propagation during crystal growth and dissolution, Nat. Mater. **14**, 780 (2015).

[16] Y. Kohmura, T. Ishikawa, H. Takano, and Y. Suzuki, Shearing x-ray interferometer with an x-ray prism, J. Appl. Phys. **93**, 2283 (2003).

[17] Y. Kohmura, T. Sakurai, T. Ishikawa, and Y. Suzuki, Phase retrieval with two-beam off-axis x-ray holography, J. Appl. Phys. **96**, 1781 (2004).

[18] Y. Kohmura, T. Sakurai, T. Ishikawa, A. Takeuchi, Y. Suzuki, and S. Goto, Determination of complex transmissivity using x-ray in-line holography and two-beam interferometry, J. Appl. Phys. **102**, 023101 (2007).

[19] K. Tamasaku, Y. Tanaka, M. Yabashi, H. Yamazaki, N. Kawamura, M. Suzuki, and T. Ishikawa, SPring-8 RIKEN beamline III for coherent x-ray optics, Nucl. Instrum. Methods Phys. Res. Sect. A **467–468**, 686 (2001).

[20] D. Takei, Y. Kohmura, Y. Senba, H. Ohashi. K. Tamasaku, and T. Ishikawa, X-ray collimation by the parabolic cylinder mirror in SPring-8/BL29XUL, J. Synchrotron Radiat. **23**, 158 (2016).

[21] T. Kameshima, A. Takeuchi, K. Uesugi, T. Kudo, Y. Kohmura, K. Tamasaku, K. Muramatsu, T. Yanagitani, M. Yabashi, and T. Hatsui, Development of an X-ray imaging detector to resolve 200 nm line-and-space patterns by using transparent ceramics layers bonded by solid-state diffusion, Opt. Lett. **44**, 1403 (2019).